Atmos. Chem. Phys. Discuss., 12, 23793–23828, 2012
www.atmos-chem-phys-discuss.net/12/23793/2012/
doi:10.5194/acpd-12-23793-2012
© Author(s) 2012. CC Attribution 3.0 License.

Atmospheric Chemistry and Physics Discussions

This discussion paper is/has been under review for the journal Atmospheric Chemistry and Physics (ACP). Please refer to the corresponding final paper in ACP if available.

Could aerosol emissions be used for regional heat wave mitigation?

D. N. Bernstein[1,2], J. D. Neelin[2], Q. B. Li[2], and D. Chen[2]

[1]Department of Soil and Water Sciences, Robert H. Smith Faculty of Agriculture, Food and Environment, The Hebrew University of Jerusalem, POB 12, Rehovot 76100, Israel
[2]Department of Atmospheric and Oceanic Sciences, University of California, Los Angeles, 405 Hilgard Ave., Los Angeles, CA 90095, USA

Received: 3 July 2012 – Accepted: 27 August 2012 – Published: 12 September 2012

Correspondence to: J. D. Neelin (neelin@atmos.ucla.edu)

Published by Copernicus Publications on behalf of the European Geosciences Union.

Abstract

Geoengineering applications by injection of sulfate aerosols into the stratosphere are under consideration as a measure of last resort to counter global warming. Here adaptation to a potential regional scale application to offset the impacts of heat waves is critically examined. The effect of regional scale sulfate aerosol emission over California in each of two days of the July 2006 heat wave using the Weather Research and Forecasting model with fully coupled chemistry (WRF-Chem) is used to quantify potential reductions in surface temperature as a function of emission rates in the lower stratosphere. Over the range considered, afternoon temperature reductions scale almost linearly with injections. Local meteorological factors yield geographical differences in surface air temperature sensitivity. For emission rates of approximately 30 $\mu g\,m^{-2}\,s^{-1}$ of sulfate aerosols (with standard WRF-Chem size distribution) over the region, temperature decreases of around 7 °C result during the middle part of the day over the Central Valley, one of the hardest hit by the heat wave. Regions more ventilated with oceanic air such as Los Angeles have slightly smaller reductions. The length of the hottest part of the day is also reduced. Advection effects on the aerosol cloud must be more carefully forecast for smaller injection regions. Verification of the impacts could be done via measurements of differences in reflected and surface downward shortwave. Such regional geoengineering applications with specific near-term target effects but smaller cost and side effects could potentially provide a means of testing larger scale applications. However, design trade-offs differ from global applications and the size of the required injections and the necessity of injection close to the target region raise substantial concerns. The evaluation of this regional scale application is thus consistent with global model evaluations emphasizing that mitigation via reduction of fossil fuels remains preferable to considering geoengineering with sulfate aerosols.

CC BY

1 Introduction

Global surface temperatures are expected to rise over the coming century due to the ongoing emission of greenhouse gases, with attendant changes in frequency of extreme events such as heat waves (IPCC, 2007). Geoengineering solutions are under discussion as a potential means of offsetting this rise. A particular solution that has been proposed includes injecting sulfate aerosols into the stratosphere and cooling the earth's surface by reflecting incoming shortwave flux. Initially proposed by Budyko (1974), this has been controversial for obvious reasons. Because the effort to reduce greenhouse gas emissions is failing the proposal has come into vogue again. Since serious consideration by Crutzen (2006), there have been a number of studies quantifying the effects of the global scale (Rasch et al., 2008; Robock et al., 2008; Brovkin et al., 2009; Jones et al., 2010; Kravitz et al., 2011; Niemeier et al., 2011; Volodin et al., 2011), and a number of studies raising substantial concerns regarding side effects (Matthews and Caldeira, 2007; Trenberth and Dai, 2007; Robock, 2008; Tilmes et al., 2008; Heckendorn et al., 2009; Kravitz et al., 2009; Robock et al., 2010). Crutzen (2006) estimated that the insertion of approximately 5 Tg per year of sulfur would be required to balance the impact of greenhouse gas warming in the case of a double-CO_2 emission scenario. Wigley (2006) suggested that an annual 5 Tg sulfur flux would be sufficient, alongside a reduction in emissions, while Pierce et al. (2010) and English et al. (2012) consider 10 $Tg\,S\,yr^{-1}$. The geoengineering injection of sulfate aerosols can be compared to those coming from a volcanic eruption. For example, Robock (2002), based on the eruption of Mount Pinatubo in June of 1991, estimated that about 20 Tg of SO_2 was released, which caused up to 2 °C of cooling in surface temperatures with Northern Hemisphere continents in the summer of 1992. Rasch et al. (2008) pointed out that the impact of the aerosol emissions depends on the size of the inserted aerosols, and that smaller-sized aerosols scatter more efficiently.

The present study is motivated by the argument that it is useful for groups whose primary research focus lies elsewhere to contribute to evaluation of potential geoengineering

ACPD
12, 23793–23828, 2012

Could aerosol emissions be used for regional heat wave mitigation?

D. N. Bernstein et al.

proposals, especially where tools developed for other purposes can contribute at low cost to particular aspects of understanding the issues involved. While sharing deep reservations regarding the wisdom of geoengineering, we here use a setup of the the Weather Research and Forecasting model with fully coupled chemistry (WRF-Chem) (Grell et al., 2009) that has been used for air quality studies over California (Chen et al., 2012) to provide a model-based evaluation of one potential application of geoengineering. It is worth underlining that the technology to do such an experiment in the real world does not currently exist, but there is active research on such methods, including patent applications (Chan et al., 2010). Given this, it is important to have model-based studies to help to put into perspective what would be implied if such methods should become available.

In particular, this study examines whether aerosol injections, specifically those which are being considered for global scale geoengineering, could be applied at the regional scale with the timing chosen to mitigate heat waves, or excessively hot weather events. If negative impacts of global warming create pressure for regional planners to enact geoengineering solutions, there are a number of factors that may bring regional scale interventions to the forefront of the debate. Regional actions might involve less concerted effort and less international cooperation than a global scale application. Because global warming is tending to affect regions differently, regional geoengineering solutions could prove more feasible than their proposed global counterparts. Finally, smaller-scale solutions could potentially provide a means of testing the larger scale applications. However, the design considerations are not exactly the same; here we consider injection of sulfate aerosols to impact shortwave radiation on a time scale less than a day in the regional application. Global applications allow for longer evolution time which may include gas phase formation of sulfate aerosols and substantial impacts of microphysical considerations including deposition (Pierce et al., 2010; English et al., 2012). The aspect of the problem considered here emphasizes advection and regional scale impacts, while using a standard source treatment from WRF-Chem.

ACPD
12, 23793–23828, 2012

Could aerosol emissions be used for regional heat wave mitigation?

D. N. Bernstein et al.

CC BY

The aim is to provide a sense of the meteorological factors that would need to be taken into account in evaluating any such potential application.

We choose the heat wave of July 2006 in California as a case study. During this abnormal event, extremely hot surface temperatures were observed, resulting in a death toll estimated to exceed 140 (Ostro et al., 2009). The heat wave lasted for 17 days and peaked on 23 July (Gershunov et al., 2009). Figure 1 shows surface air temperatures simulated by the WRF model for 22 July and 23 July, as detailed in Sect. 3. The simulated highest temperatures in California were in a narrow region in the Central Valley between the ventilated coastal area and mountain ridge (see the Supplement for surface air temperatures and upper-level flow patterns from the North American Regional Reanalysis, Messinger et al., 2006). The upper-level flow field is northerly over much of the domain at 200 mbar with speeds ranging from roughly 4 to 14 $m s^{-1}$ over California. Heat waves may not evolve in exactly the same manner in future climate. However, the example of the recent heat wave serves to provide an upper-level flow field of reasonable magnitude and pattern, which is important to the advection of emitted aerosols, and a temperature simulation that yields high temperatures in a geographic pattern that is meteorologically reasonable.

The first point to address is whether advection rapidly carries the emitted aerosols away from the target region. Subsequent points of examination are quantifying the potential size of the reduction in surface solar radiation and reduction in surface air temperature (relative to the control simulation) for a given size of injection, and whether the meteorology of certain regions makes such experiments more or less effective.

2 Setup and experiments

The Weather Research and Forecasting model with fully coupled chemistry (WRF-Chem) Grell et al. (2009); Grell (2008); Grell et al. (2011) is applied to simulate the impact of low stratospheric sulfate aerosols. The WRF-Chem is a nonhydrostatic mesoscale model that uses a terrain-following, hydrostatic-pressure vertical coordinate with

ACPD
12, 23793–23828, 2012

the top of the model being a constant pressure surface. The horizontal structure of the model grid is the Arakawa-C grid. Here, the time integration scheme in the model uses a third-order Runge-Kutta scheme. The Yonsei University scheme (YSU, Hong et al., 2004) is used to parametrize the planetary boundary layer and Grell 3D ensemble scheme (Grell and Devenyi, 2002) for convective parameterization. The NOAA land-surface model (Chen and Dudhia, 2001) is used. The chemistry package includes dry deposition, aqueous phase chemistry coupled to some of the microphysics and aerosol schemes, biogenic emissions, anthropogenic emissions, chemical mechanisms, photolysis schemes, and aerosol schemes (Grell et al., 2009; Fast et al., 2006; Zaveri et al., 2008). The Model for Simulating Aerosol Interactions and Chemistry (MOSAIC) (Fast et al., 2006; Zaveri et al., 2008; Barnard et al., 2010) has been used for aerosol treatment. MOSAIC distributes aerosols according to their dry size into the discrete bins and calculates the mass and number for each bin. The standard option, four bins (0.039–0.156, 0.156–0.625, 0.625–2.5, 2.5–10.0 µm dry diameter) is used. The relevant aerosol species here is sulfate (SULF = $SO_4^{2-} + HSO_4^-$). The size bins are defined by their lower and upper dry particle diameter, so water uptake or loss does not transfer particles between bins (Zaveri et al., 2008). Only the Wexler et al. (1994) parameterization of $H_2SO_4{-}H_2O$ homogeneous nucleation is used in the MOSAIC (Zaveri et al., 2008). Transfer of the mass between size bins and particle growth due to condensation and coagulation is computed using the two-moment approach described by Tzivion et al. (1989). The aerosol optical properties, such as extinction, single-scattering albedo, and the asymmetry factor for scattering, are calculated as a function of wavelength and three-dimensional position. The refractive index, which is associated for each chemical constituent of the aerosol, is calculated by volume averaging for each size bin, and Mie theory is used to estimate the extinction efficiency and the scattering efficiency. For efficient computation of the extinction and the scattering efficiencies, WRF-Chem uses a methodology described by Ghan et al. (2001). After the aerosol radiative properties are calculated they are used in the shortwave radiative transfer model. A Dudhia shortwave

ACPD
12, 23793–23828, 2012

CC BY

radiative scheme is applied in our study to calculate the downward solar radiation flux, taking into account the diurnal variation of the solar zenith angle (Dudhia, 1989).

For this study we use version 3.1.1 of WRF-Chem, using the two-way nest option to increase resolution in an inner domain. The coarse model domain is configured covering the Western United States with a horizontal resolution of 36 km and 80 × 60 grid points, and the fine domain of California and Nevada with a horizontal resolution of 12 km and 97 × 97 grid points. The fine domain corresponds to the area shown in Fig. 1. The vertical structure of the model is 28 grid points with the top of the model at 50 hPa. The initial and lateral boundary conditions for meteorological variables are obtained from the National Centers for Environmental Prediction Eta/North American Mesoscale model data set with 40 km spatial resolution at three-hour intervals (available from the Research Data Archive dataset number ds609.2 maintained at the National Center for Atmospheric Research http://dss.ucar.edu). Sea surface temperatures are specified from the same data set. The WRF-Chem emissions for all anthropogenic chemical species is based on the EPA 2005 National Emission Inventory (NEI 05). This setup follows the same model configuration as is validated by Chen et al. (2012) during a field campaign in May 2010 in California. A similar configuration of WRF over California is used in several studies and evaluated against observations for various events (Bao et al., 2008; Lu et al., 2012). Chapman et al. (2009) used WRF-Chem with the MOSAIC aerosol scheme to study the radiative impact of elevated point sources, which showed good agreement with observed data.

In for the set of model experiments considered here, we directly inject sulfate aerosols into the lower stratosphere (a single model level at an altitude discussed below) over an idealized region which varies with the experiment. The sulfate aerosols are distributed into the 4 MOSAIC size bins following size distribution prescribed in the standard simulation (Fast et al., 2006; Zaveri et al., 2008). In the discussion below we will summarize the sulfate aerosol emission rates for this stratospheric injection in mass units, $\mu g\, m^{-2}\, s^{-1}$, noting that the associated number concentration distributions are computed according to the standard model treatment for surface sulfate aerosol emissions. The

ACPD
12, 23793–23828, 2012

CC BY

emissions are done on the 12 km fine grid over the specified subdomain in each experiment. The evolution of the bin distribution and aerosol growth will be discussed in Sect. 3.3.

We perform sets of experiments in which the rate of emission of sulfate aerosols per unit area and the size of the geographic area over which injection is assumed to occur are varied, respectively, as summarized in Table 1. In each case the injection is done over an area of idealized spatial shape, and the sequence of experiments moves from what we term a large-scale injection region that covers all of California (plus some surrounding regions) to successively smaller scales. Injection areas roughly corresponding to the size of Southern California and the San Joaquin Valley are referred to as regional scale, while the smallest injection areas considered here, equivalent to 48 × 36 km, correspond to roughly a metropolitan scale. One of the main effects to be illustrated in the sequence of smaller areas is the impact of advection effects and mixing effects from the edges of the injection region as a function of scale, while noting the trade-off associated with the total mass of injected aerosol required for each experiment. The evaluation over the large-scale area permits the impacts on surface temperature to be evaluated as a function of emission rate per unit area in a context where horizontal mixing edge effects are relatively small. It further permits local sensitivity of the surface response to a relatively homogeneous aerosol cloud to be seen.

The set of experiments varying sulfate aerosol emission rates over a range (6, 10, 20, 30, and 60 $\mu g\,m^{-2}\,s^{-1}$) is performed using the large-scale injection area to evaluate the impact of the magnitude of the emission rate, as well as the local sensitivity within this region. Results at example grid points, one in the Los Angeles region (34.05° N; 118.25° W) and another in the Central Valley region (Fresno, 36.75° N; 119.77° W), are seen as a function of the emission rate in Fig. 2. For the figures presented throughout, we have chosen the experiment with emissions rate of 30 $\mu g\,m^{-2}\,s^{-1}$ as typifying the results (termed the large-scale illustration case in Table 1). Given the magnitude of the surface temperature response (around 6 °C at the time shown in Fig. 2), this may be higher than would be required if such experiments were to be taken to a real-world

ACPD
12, 23793–23828, 2012

CC BY

application, but it produces a signal strong enough to be well above the level of numerical noise in the simulated response. Similar spatial patterns to those presented below are found in all the large-scale experiments, with amplitude proportional to the emission rate. The amplitude of the injections will be discussed in more detail in Sect. 3.2. For the time of the aerosol injection, we have chosen a two-hour period in the morning, from 06:00 LT to 08:00 LT local time, so we can see the effect of the aerosols on the full diurnal cycle. The experiment is repeated independently on each of two days of the heat wave (22 July and 23 July 2006), as discussed in Sect. 3.3.

3 Large-scale idealized experiment

3.1 Advective effect

Figures 3 and 4 show the spatial patterns of sulfate aerosol mixing ratio for a key size bin, bin 2 (chosen for its close relationship to shortwave impact in Fig. 2), evolving as a function of time on 22 July and 23 July from emission in a simple square shape, for the large-scale injection experiment illustration case. Injection over such a large-scale region would likely be impractical for any real-world application but this experiment serves to illustrate regional differences in the temperature response under an area of relatively similar solar response. A first point from Fig. 3 is that advection does not rapidly carry the aerosol cloud outside of the domain, even for injections in the lower stratosphere. Figure 3 also demonstrates the importance of vertical advection, not just horizontal, leading to the inhomogeneities in the concentrations inside of the injections square. Furthermore, the level of aerosol injection has been chosen according to meteorology, an example of a strategy that can be advantageous to the regional application for each particular heat wave event. We chose the level of 12 km as the level of aerosol injection, which has a relatively low wind speed, as estimated from the morning wind values over an important target region, Los Angeles. This helps reduce the rate at which the aerosol cloud is advected. This altitude is just above the cold-point tropopause – a level

ACPD
12, 23793–23828, 2012

CC BY

lower than would be typically chosen for a global application – and so also serves to illustrate a trade-off discussed in Sect. 6.

3.2 Amplitude of the emissions

Figure 2 shows each bin mixing ratio together with surface temperature and surface shortwave radiation differences as a function of aerosol emissions for the two sample locations. For both regions, there is a highly linear relation between emissions, sulfate mixing ratios in bin 2 and shortwave radiation differences, although the temperature response curve differs from one region to another. The temperature response curve has a linear relation with bin 2 mixing ratios and shortwave differences in the Central Valley area, reaching a reduction of about 11 °C in the case of a 60 $\mu g\,m^{-2}\,s^{-1}$ aerosol injection. In the Los Angeles area, the temperature response increases in the case of an aerosol emission higher than 6 $\mu g\,m^{-2}\,s^{-1}$ and achieves a maximum of 8 °C in the case of the highest aerosol emission rate. Each of the bin mixing ratio curves behaves similarly in the two locations. The mixing ratio curve of the first bin, which has the finest particles, increases and stabilizes after reaching 22 $\mu g\,kg^{-1}$ of dry air at an aerosol emission of 6 $\mu g\,m^{-2}\,s^{-1}$. The mixing ratio curve of bin 3 increases, since the aerosol emission is higher than 6 $\mu g\,m^{-2}\,s^{-1}$. The mixing ratio of bin 4 is very low but shows a slight increase with aerosol emission increases. For the case of 30 $\mu g\,m^{-2}\,s^{-1}$ aerosol emission, the shortwave reduction of about 200 $W\,m^{-2}$ corresponds to approximately a 18 % reduction in incoming surface shortwave relative to the control.

3.3 Shortwave radiation and temperature for large-scale injection case

Figures 5 and 6 show the downward surface shortwave response at times corresponding to Figs. 3 and 4, respectively. In the middle of the day, the overall size of the impact is a decrease of about 350 $W\,m^{-2}$. Aerosols were injected during morning hours, between 06:00 LT and 08:00 LT. The selection of time for inserting aerosols depends on their not being carried out of the target region too quickly. Inserting them in the early-morning

CC BY

allows them more time to act before reaching the time of maximum temperature and aids examination of impact on the diurnal cycle.

The impact of these shortwave reductions by the aerosol cloud for surface air temperature may be seen in Figs. 7 and 8. For the chosen rate of emissions in this experiment, the impacts are substantial. Regional differences in the sensitivity of the response may be noted. One example is the greater Los Angeles region, which has less impact for a given level of sulfate aerosol concentrations than does the Central Valley. This appears to be consistent with the fact that the Los Angeles region tends to be strongly ventilated by wind flow from the ocean, while the Central Valley's maximum temperatures tend to be strongly affected by local balances involving radiative transfer and boundary layer turbulence.

Comparing the runs for 22 July and 23 July indicates the modest effects of slightly different day to day flow patterns within the heat wave (23 July was slightly hotter than 22 July). The results of sulfate mixing ratio, downward shortwave flux differences, and surface air temperature are shown in Figs. 4, 8, and 6, respectively. The overall simulations for both days show a very similar pattern of surface shortwave and surface temperature differences. The simulations of both days show significantly higher temperature differences in the Central Valley, and the surface air temperature difference in the middle of the day reaches up to 7 °C in that area. Thus to a first approximation, the shortwave and temperature differences may be taken as typical of what would result for other similar heat wave days in this region.

On both days, the surface air temperature changes are actually larger at the time of the morning temperature increase and the evening temperature decrease, which can be understood by examining the evolution through the course of the day.

As a prelude to this, Fig. 9 shows the sulfate aerosol mixing ratio of each size bin and aerosol number for each bin changing with time in the Los Angeles and the Central Valley areas. Rapid increase in the smallest-sized bin 1 is seen during the two hours of the injection, followed by an ongoing decrease after the end of injection in the second hour. The bin 2 mixing ratio increases for another two hours after the injection,

ACPD
12, 23793–23828, 2012

Could aerosol emissions be used for regional heat wave mitigation?

D. N. Bernstein et al.

associated with the conversion from bin 1 to 2. Bins 3 and 4 increase slowly with time and tending to stabilize several hours after the injection.

The downward shortwave radiation and surface temperature differences time-series are shown in Fig. 10 for the Los Angeles and the Central Valley areas for both 22 July and 23 July. The pattern of shortwave differences is similar for both days and for both areas. In each case, the shortwave reduction is slightly larger around 09:00 LT and 17:00 LT due to variation of total optical depth through the cloud with solar zenith angle. The temperature impact differs from the Los Angeles to the Central Valley areas. The Central Valley surface temperature impact has two clear peaks. One peak, of about 16 to 17 °C, occurs in the morning at 09:00 LT, while the other peak, which reaches 19 to 21 °C, occurs in the evening at 18:00 LT. The Los Angeles temperature impact has a peak of 7.5 to 9 °C at 09:00 LT and another minor peak of about 5 °C at 19:00 LT. In each case, the large peak in the difference corresponds to the time of rapid increase or decrease of total temperature at the beginning or end of the day, effectively shortening the hot part of the day. In the Central Valley, the local meteorological balances in the control run yield the hottest part of the day in late afternoon, followed by a rapid drop in temperature, while in the experiment this is reduced by 7 °C, followed by an earlier drop in temperature. In Los Angeles, the lag of the hot part of the day, and the subsequent temperature drop, are each smaller, and the reduction of temperature more constant in the experiment.

4 Smaller scale injection regions

The large-scale idealized experiment serves to highlight regional differences in sensitivity and to provide a sense of the magnitude of temperature response for a given level of aerosol loading, but involves far larger injection areas than would be under consideration for any practical implementation. We thus consider examples that move towards more localized injection regions. For efficiency of presentation, we show two localized regions in a single experiment. For the regional scale experiments, we specify

ACPD
12, 23793–23828, 2012

one injection region over Southern California area and another one over the southern part of San Joaquin Valley, which is part of the Central Valley. The initial area coverage of the two regional scale injection regions is $69 \times 10^3\,\text{km}^2$ and $48 \times 10^3\,\text{km}^2$, respectively. The smaller is roughly 1/22 the size of the large-scale experiment injection area (the two together total about 1/9 of the large-scale experiment). These are each larger than would be used in a practical application, but serve to illustrate the challenges that would arise at a regional scale. In particular, advective effects will become increasingly important to take into account with respect to specific target regions.

Here the examples provide shading, (i) to a region extending from the greater Los Angeles metropolitan area down to San Diego and a large region to the east, and (ii) to a region surrounding Fresno in the Central Valley and extending down to San Bernardino. It would be possible to tailor such regions more specifically to populated or agricultural areas, or to undertake continuous injections upstream of the region. The latter would have the trade-off for a given amount of total injections of spreading the injections over a longer time interval. For simplicity, the example here is done with two hours of injections in the morning, as in the large-scale experiment, with the injection location and areal extent being estimated such that the cloud covers much of the target region for most of the day, even taking into account the advective movement. We use simple rectangular injection regions so it is easy to visualize the impact of advection, but of course this would be optimized in any practical application using weather forecasts for wind fields. The estimates here use 12 hour back trajectories from the HYbrid Single-Particle Lagrangian Integrated Trajectory (HYSPLIT) model (Draxler and Rolph, 2012).

Figures 11 and 12 show the surface shortwave and surface air temperature differences relative to the control resulting from these injection patterns. At 10:00 LT, which is four hours after the injection, the cloud still resembles a slightly shifted and stretched version of the rectangular initial region. At 16:00 LT, the area of the aerosol cloud has altered substantially but in a manner that is largely predictable from the flow field. In this test, we choose an initial injection region such that the cloud would not drift over

ACPD
12, 23793–23828, 2012

Could aerosol emissions be used for regional heat wave mitigation?

D. N. Bernstein et al.

Discussion Paper | Discussion Paper | Discussion Paper | Discussion Paper |

the ocean within 12 hours, although some part of the cloud covers unpopulated areas over the desert. From the evolution of the short wave pattern in Fig. 11, one can infer that coverage for an area comparable to Los Angeles could plausibly be achieved with overall injections one quarter to one tenth the size, although this would require careful consideration of the flow pattern.

The amplitude of the shortwave difference and surface air temperature differences within each region are very similar to those in the large-scale area test shown in Figs. 5 and 7, but the values of shortwave and surface air temperature are slightly smaller due to the mixing of clean air from outside the cloud.

Smaller metropolitan and targeted agricultural injection areas both of $1.7 \times 10^3\,km^2$ are chosen to illustrate the impacts of advection and mixing as one moves further down in horizontal scale. One area covers Los Angeles metropolitan area and another one covers agricultural area over Fresno. Because the aerosol cloud travels further relative to its horizontal dimension, we also illustrate the impact of injection time chosen later in the day, which reduces the prediction problem of the path the cloud will travel toward a desired target region. Injection here is done from 11:00–13:00 LT. Figure 14 shows the surface air temperature and surface shortwave flux differences at 14:00 LT and 16:00 LT relative to the control. Surface air temperature and surface shortwave flux differences tend to be smaller than the response in comparable areas in the experiments with larger injection areas shown in Figs. 5c, d, 7c, d, 11c, d and 12c, d. At this scale, the edge effects are becoming sufficiently important that even the response under the center of the cloud is not reaching the full response that would occur for larger area coverage.

With these trade-offs in mind, the total mass of aerosol injected provides some perspective on the magnitude of the endeavor that would be implied by the different horizontal scales. The injection area that covers the Southern California area corresponds to approximately 15 Gg of sulfate aerosols or 3.75 Gg of sulfur [2 Tg SO_2 = 1 Tg S ~ 4 Tg aerosol particles (Rasch et al., 2008a)] integrated over the region and over the two-hour injections interval for a given day. Compared to the 10 Tg S annual injection under recent consideration for global geoengineering applications (Pierce et al., 2010; English

ACPD
12, 23793–23828, 2012

Could aerosol emissions be used for regional heat wave mitigation?

D. N. Bernstein et al.

et al., 2012), this is a small fraction: roughly 1/2700th the size in terms of sulfur equivalent. However, to provide a rough visualization of the mass of sulfate aerosols involved, this corresponds to a payload of about 120 C-5s, the largest US cargo jets, i.e. a very substantial mass. The Los Angeles metropolitan injection area roughly corresponds to 0.36 Gg of sulfate aerosol emitted over the two-hour interval, i.e. to approximately the payload of 3 C-5s (roughly 10^{-5} of the sulfur equivalent of the global case). It must be underlined that this amount is for just one day, for one heat wave, and for the one specific region.

5 Testing via shortwave measurements

In considering how one might test the effectiveness of such aerosol injections in a real-world experiment, the natural variability of temperature and the fact there is no control experiment must be taken into account. There would be no way of telling what temperature would have occurred in the absence of the aerosol release (Robock et al., 2010). However downward shortwave reductions, such as those shown in Figs. 5 and 11 and the corresponding upward reflected solar at the top of the atmosphere, could be directly measured. The aerosol cloud spatial pattern is initially highly identifiable and can be tracked through time. This process would be made easier in this application because heat waves tend to occur at times with small cloud cover. In conjunction with other measurements, the shortwave reduction could be attributed to the injections with fairly high accuracy, and this can be used as the leading benchmark of the impact. To translate this to surface temperature reductions, one would then use data sets from comparable meteorological situations but with and without natural cloud cover to estimate the surface temperature reduction per decrease in surface shortwave flux.

ACPD
12, 23793–23828, 2012

Could aerosol emissions be used for regional heat wave mitigation?

D. N. Bernstein et al.

cc BY

6 Discussion and conclusions

This study critically examines the potential for an aerosol-injection geoengineering strategy to be applied at a regional scale to reduce the impacts of a heat wave. If geoengineering proposals come to be taken seriously at the global scale, there may be increasing motivation to consider regional applications, and so it is worth assessing in advance the size of the emission required to have a regional impact, and the likely trade-offs and concerns. The sensitivity of surface temperature and the advection effects at the altitude of injection will both depend on the meteorology of the particular heat wave. Thus a specific example is examined for the conditions of an observed heat wave with a regional scale model to provide a sense of how substantial these effects will be.

The results indicate that a sufficiently large emission of sulfate aerosols can indeed have a substantial impact on surface air temperature, although the temperature response varies among areas. For instance, temperature response in the Central Valley is larger than that in the Los Angeles area. This is partially attributable to the topographical locations of the Central Valley and Los Angeles, as well as Los Angeles' close proximity to the Pacific Ocean, and was reproducible on both days of the 2006 heat wave. The temperature response during the hottest part of the day is a key factor in reducing heat wave impacts, and is roughly 7 °C in the Central Valley for the case of an emission of 30 $\mu g\,m^{-2}\,s^{-1}$. The temperature difference has a strong diurnal cycle, and is actually larger during the morning and late afternoon hours, due to the optical depth dependence on solar zenith angle. This has the effect of shortening the hot part of the day.

The temperature reduction scales approximately linearly with the magnitude of the aerosol injection, so the latter could be reduced to meet temperature targets. The flow field at the height of injection is a significant factor in the evolution of the aerosol cloud. Thus, the choice of the injection amplitude and height level would depend on the meteorology at the time of the heat wave. These appear to be within the realm that could

ACPD
12, 23793–23828, 2012

CC BY

be addressed by forecasting the flow, provided the injections would be carried out over regions at least as large as a greater metropolitan area. The choice of the height of the injection based on flow field characteristics would yield a trade-off relative to choices that might be made for maximizing global scale impacts or minimizing downstream side effects. The case presented here uses a choice that might typify that of a decision-maker choosing the injection height based solely on local considerations of minimal flow for a specific city at a time just before the start of the injections. The height used for illustration in this case is just above the cold-point tropopause, where the winds were relatively weak over Los Angeles for this case. This is at lower altitude than would be optimal from the perspective of global dispersion and of minimizing reentry into the troposphere in states downstream. This serves to illustrate that if such an approach were to be considered for actual application, there would need to be requirements established that those responsible for local injections decisions consider the downstream effects.

For the injection area covering most of Southern California considered in Sect. 4, the sulfur equivalent of the aerosol injections on a given day is roughly 2700 times smaller than the 10 Tg annual injection of sulfur being considered for global applications. Even for smaller areas, this would represent a very substantial amount of aerosol to be lofted. Furthermore, this would have to be done repeatedly at each heat wave, and for each region. If one were in a situation of being committed to global geoengineering, the regional application might be worth consideration either as a means of testing the global application, or of timing the injection to produce additional regional benefit in terms of temperature reduction during heat waves. Otherwise, regional planners might be well advised to consider other strategies involving regional adaptation of infrastructure to protect against heat wave impacts.

This is reinforced by the fact that, in addition to potential negative downstream impacts such as on precipitation, or ozone layer depletion (e.g. Robock, 2008), the regional application has an additional, very substantial potential downside. To protect a populated region from the effects of the heat wave using such a method, the injections

ACPD
12, 23793–23828, 2012

would have to be conducted over or just upstream from the populated area. This immediately raises the attendant concern for possible local negative effects or the public perception of these effects. Considerations for the local safety of the emission process would be much greater than those potentially arising from injections over a remote, unpopulated region, as could be done for global geoengineering applications.

Thus while a regional scale application may have sufficient appeal to make it worth assessing in model simulations, the considerations noted here are consistent with recommendations from assessment of global scale applications (Robock et al., 2008; Heckendorn et al., 2009; English et al., 2012) that the downsides of geoengineering with sulfate aerosols prevent considering them a good alternative to mitigation via reduction of fossil fuel emissions.

Supplementary material related to this article is available online at: http://www.atmos-chem-phys-discuss.net/12/23793/2012/acpd-12-23793-2012-supplement.pdf.

Acknowledgements. We thank A. Robock for discussion and J. E. Meyerson for graphical assistance. We also gratefully acknowledge the NOAA Air Resources Laboratory (ARL) for the provision of the HYSPLIT transport and dispersion model used in this publication. This study was supported by National Science Foundation Grant AGS-1102838.

References

Bao, J. W., Michelson, S. A., Persson, P. O. G., Djalalova, I. V., and Wilczak, J. M.: Observed and WRF-simulated low-level winds in a high-Ozone episode during the Central California ozone study, J. Appl. Meteorol. Clim., 47, 2372–2394, 2008. 23799

Barnard, J. C., Fast, J. D., Paredes-Miranda, G., Arnott, W. P., and Laskin, A.: Technical Note: Evaluation of the WRF-Chem "Aerosol Chemical to Aerosol Optical Properties" Module using data from the MILAGRO campaign, Atmos. Chem. Phys., 10, 7325–7340, doi:10.5194/acp-10-7325-2010, 2010. 23798

ACPD
12, 23793–23828, 2012

Could aerosol emissions be used for regional heat wave mitigation?

D. N. Bernstein et al.

CC BY

Brovkin, V., Petoukhov, V., Claussen, M., Bauer, E., Archer, D., and Jaeger, C.: Geoengineering climate by stratospheric sulfur injections: earth system vulnerability to technological failure, Climatic Change, 92, 243–259, 2009. 23795

Budyko, M. I.: Climate and Life. Academic Press, New York, USA, 508 pp., 1974. 23795

Chan, A. K., Hyde, R. A., Myhrvold, N. P., Tegreene, C. T., and Wood, L. L.: High altitude atmospheric injection system and method, US Patent Application Publication: US 2010/0071771, Publication Date: 25 March 2010. 23796

Chapman, E. G., Gustafson Jr., W. I., Easter, R. C., Barnard, J. C., Ghan, S. J., Pekour, M. S., and Fast, J. D.: Coupling aerosol-cloud-radiative processes in the WRF-Chem model: Investigating the radiative impact of elevated point sources, Atmos. Chem. Phys., 9, 945–964, doi:10.5194/acp-9-945-2009, 2009. 23799

Chen, D., Li, Q., Fovell, R. G., Li, Z., Stutz, J., Mao, Y., Zhang, L., Pikelnaya, O., Tsai, J. Y., Haman, C., Lefer, B., de Gouw, J., Holloway, J., Murakami, J., and Ryerson, T.: WRF-Chem simulation of meteorology and CO in the Los Angeles basin during CalNex-2010, J. Geophys. Res., to be submitted, 2012. 23796, 23799

Chen, F. and Dudhia, J.: Coupling an advanced land-surface (hydrology model with the Penn State (NCAR MM5 modeling system. Part I: Model description and implementation, Mon. Weather Rev., 129, 569–585, doi:10.1175/1520-0493(2001)129<0569:CAALSH>2.0.CO;2, 2001. 23798

Crutzen, P. J.: Albedo enhancement by stratospheric sulfur injections: a contribution to resolve a policy dilemma?, Climatic Change, 77, 211–220, 2006. 23795

Draxler, R. R. and Rolph, G. D.: HYSPLIT (HYbrid Single-Particle Lagrangian Integrated Trajectory) Model access via NOAA ARL READY Website (http://ready.arl.noaa.gov/HYSPLIT.php, last access: 2 March 2012), NOAA Air Resources Laboratory, Silver. Spring, MD, 2012. 23805

Dudhia, J.: Numerical study of convection observed during the winter monsoon experiment using a mesoscale two-dimensional model, J. Atmos. Sci., 46, 3077–3107, 1989. 23799

English, J. M., Toon, O. B., and Mills, M. J.: Microphysical simulations of sulfur burdens from stratospheric sulfur geoengineering, Atmos. Chem. Phys., 12, 4775–4793, doi:10.5194/acp-12-4775-2012, 2012. 23795, 23796, 23806, 23810

Fast, J. D., Gustafson Jr., W. I., Easter, R. C., Zaveri, R. A., Barnard, J. C., Chapman, E. G., Grell, G. A., and Peckham, S. E.: Evolution of ozone, particulates, and aerosol direct radiative

CC BY

forcing in the vicinity of Houston using a fully coupled meteorology-chemistry-aerosol model, J. Geophys. Res., 111, D21305, 2006. 23798, 23799

Gershunov, A., Cayan, D. R., and Iacobellis, S. F.: The great 2006 heat wave over California and Nevada: signal of an increasing trend, J. Climate, 22, 6181–6203, 2005. 23797

Ghan, S., Laulainen, N., Easter, R., Wagener, R., Nemesure, S., Chapman, Y., Zhang, E., and Leung, R.: Evaluation of aerosol direct radiative forcing in MIRAGE, J. Geophys. Res., 106, 5295–5316, 2001. 23798

Grell, G. A.: Coupled weather chemistry modeling, in: Large-Scale Disasters: Prediction, Control, Mitigation, edited by: M. Gad-el-Hak, Cambridge University Press, 302–317, 2008. 23797

Grell, G. A. and Devenyi, D.: A generalized approach to parameterizing convection combining ensemble and data assimilation techniques, Geophys. Res. Lett., 29, 1693, doi:10.1029/2002GL015311, 2002. 23798

Grell, G. A., Peckham, S. E., Schmitz, R., McKeen, S. A., Frost, G., Skamarock, W. C., and Eder, B.: Fully coupled "online" chemistry within the WRF model, Atmos. Environ., 37, 6957–6975, 2009. 23796, 23797, 23798

Grell, G. A., Fast, J. D., Gustafson, Jr., W. I., Peckham, S. E., McKeen, S. A., Salzmann, M., and Freitas, S.: On-line chemistry within WRF: description and evaluation of a State-of-the-Art multiscale air quality and weather prediction model, in: Integrated Systems of Meso-Meteorological and Chemical Transport Models, edited by: Baklanov, A., Mahura, A., and Sokhi, R., Springer, Heidelberg, Germany, 41–54, 2011. 23797

Heckendorn, P., Weisenstein, D., Fueglistaler, S., Luo, B. P., Rozanov, E., Schraner, M., Thomason, L. W., and Peter, T.: The impact of geoengineering aerosols on stratospheric temperature and ozone, Environ. Res. Lett., 4, 045108, 2009. 23795, 23810

Hong, S.-Y., Dudhia, J., and Chen, H.-S.: A revised approach to ice microphysical processes for the bulk parameterization of clouds and precipitation, Mon. Weather Rev., 132, 103–120, 2004. 23798

Jones, A., Haywood, J., Boucher, O., Kravitz, B., and Robock, A.: Geoengineering by stratospheric SO2 injection: results from the Met Office HadGEM2 climate model and comparison with the Goddard Institute for Space Studies ModelE, Atmos. Chem. Phys., 10, 5999–6006, doi:10.5194/acp-10-5999-2010, 2010. 23795

Intergovernmental Panel on Climate Change: Contribution of Working Group I to the Fourth Assessment Report of the Intergovernmental Panel on Climate Change, Climate Change 2007:

CC BY

The Physical Science Basis, edited by: Solomon, S., Qin, D., Manning, M., Chen, Z., Marquis, M., Averyt, K. B., Tignor, M., and Miller, H. L., Cambridge University Press, Cambridge, UK, 2007. 23795

Klemp, J. B., Skamarock, W. C., and Dudhia, J.: Conservative split-explicit time integration methods for the compressible nonhydrostatic equations, Mon. Weather Rev., 135, 2897–2913, 2007.

Kravitz, B., Robock, A., Oman, L., Stenchikov, G., and Marquardt, A. B.: Sulfuric acid deposition from stratospheric geoengineering with sulfate aerosols, J. Geophys. Res., 114, D14109, 2009. 23795

Kravitz, B., Robock, A., Boucher, O., Schmidt, H., Taylor, K. E., Stenchikov, G., and Schulz, M.: The Geoengineering Model Intercomparison Project (GeoMIP), Atmos. Sci. Lett., 12, 162–167, 2011. 23795

Lu, W., Zhong, S., Charney, J. J., Bian, X., and Liu, S.: WRF simulation over complex terrain during a southern California wildfire event, J. Geophys. Res., 117, D05125, 2012. 23799

Matthews, H. D. and Caldeira, K.: Transient climate–carbon simulations of planetary geoengineering, P. Natl. Acad. Sci. USA, 104, 9949–9954, 2007. 23795

Mesinger, F., Dimego, G., Kalnay, E., Mitchell, K., Shafran, P. C., Ebisuzaki, W., Jovi, D., Woollen, J., Rogers, E., Berbery, E. H., Ek, M. B., Fan, Y., Grumbine, R., Higgins, W., Li, H., Lin, Y., Manikin, G., Parrish, D., and Shi, W.: North American regional reanalysis, B. Am. Meteorol. Soc., 87, 343–360, doi:10.1175/BAMS-87-3-343, 2006. 23797

Niemeier, U., Schmidt, H., and Timmreck, C.: The dependency of geoengineered sulfate aerosol on the emission strategy, Atmos. Sci. Lett., 12, 189–194, 2011. 23795

Ostro, B. D., Roth, L. A., Green, R. S., and Basu, R.: Estimating the mortality effect of the July 2006 California heat wave, Environ. Res., 109, 614–619, 2009. 23797

Pierce, J. R., Weisenstein, D. K., Heckendorn, P., Peter, T., and Keith, D. W.: Efficient formation of stratospheric aerosol for climate engineering by emission of condensible vapor from aircraft, Geophys. Res. Lett., 37, L18805, doi:10.1029/2010GL043975, 2010. 23795, 23796, 23806

Rasch, P. J., Crutzen, P. J., and Coleman, D. B.: Exploring the geoengineering of climate using stratospheric sulfate aerosols: the role of particle size, Geophys. Res. Lett., 35, L02809, 2008a. 23795

ACPD
12, 23793–23828, 2012

Could aerosol emissions be used for regional heat wave mitigation?

D. N. Bernstein et al.

cc BY

Rasch, P. J., Tilmes, S., Turco, R. P., Robock, A., Oman, L., Chen, C., Stenchikov, G. L., and Garcia, R. R.: An overview of geoengineering of climate using stratospheric sulphate aerosols, Philos. T. Roy. Soc. A, 366, 4007–4037, 2008b. 23806

Robock, A.: The climatic aftermath, Science, 295, 1242–1244, 2002. 23795

Robock, A.: 20 reasons why geoengineering may be a bad idea, B. Am. Meteorol. Soc., 64, 14–18, 2008. 23795, 23809

Robock, A., Oman, L., and Stenchikov, G. L.: Regional climate responses to geoengineering with tropical and Arctic SO_2 injections, J. Geophys. Res., 113, D16101, doi:10.1029/2008JD010050, 2008. 23795, 23810

Robock, A., Marquardt, A., Kravitz, B., and Stenchikov, G.: Benefits, risks, and costs of stratospheric geoengineering, Geophys. Res. Lett., 36, L19703, 2009.

Robock, A., Bunzl, M., Kravitz, B., and Stenchikov, G. L.: A test for geoengineering?, Science, 327, 530–531, 2010. 23795, 23807

Tilmes, S., Müller, R., and Salawitch, R.: The sensitivity of polar ozone depletion to proposed geoengineering schemes, Science, 320, 1201–1204, 2008. 23795

Trenberth, K. E. and Dai, A.: Effects of Mount Pinatubo volcanic eruption on the hydrological cycle as an analog of geoengineering, Geophys. Res. Lett., 34, L15702, doi:10.1029/2007GL030524, 2007. 23795

Tzivion, S., Feingold, G., and Levin, Z.: The evolution of raindrop spectra. Part II: collisional collection/breakup and evaporation in a rainshaft, J. Atmos. Sci., 46, 3312–3327, 1989. 23798

Volodin, E. M., Kostrykin, S. V., and Ryaboshapko, A. G.: Climate response to aerosol injection at different stratospheric locations, Atmos. Sci. Lett., 12, 381–385, 2011. 23795

Wexler, A. S., Lurmann, F. W., and Seinfeld, J. H.: Modelling urban and regional aerosols. Part I: Model development, Atmos. Environ., 28, 531–546, 1994. 23798

Wigley, T. M. L.: A Combined mitigation/geoengineering approach to climate stabilization, Science, 314, 452–454, 2006. 23795

Zaveri, R. A., Easter, R. C., Fast, J. D., and Peters, L. K.: Model for Simulating Aerosol Interactions and Chemistry (MOSAIC), J. Geophys. Res., 113, D13204, doi:10.1029/2007JD008782, 2008. 23798, 23799

ACPD
12, 23793–23828, 2012

cc BY

Table 1. Description of the experiments and their purposes as discussed in Sects. 3 and 4. Asterisk denotes the case used to illustrate spatial patterns in Figs. 3–8.

Experiment name	Emis. area [km^2]	Emis. rate [$\mu g\,m^{-2}\,s^{-1}$]	Purpose
Large-Scale	1×10^6	6; 10; 20; 30*; 60	Evaluate scaling of response with emission rate over region.
Large-Scale illustration case*	1×10^6	30	Evaluate local sensitivity over region with approximately homogeneous cloud.
Regional Scale (SoCal; San Joaquin Valley cases)	69×10^3; 48×10^3	30	Evaluate advection effects for regional scale injections.
Metropolitan or targeted agricultural scale	1.7×10^3; 1.7×10^3	30	Evaluate advection effects for smaller horizontal scale injections.

ACPD
12, 23793–23828, 2012

Could aerosol emissions be used for regional heat wave mitigation?

D. N. Bernstein et al.

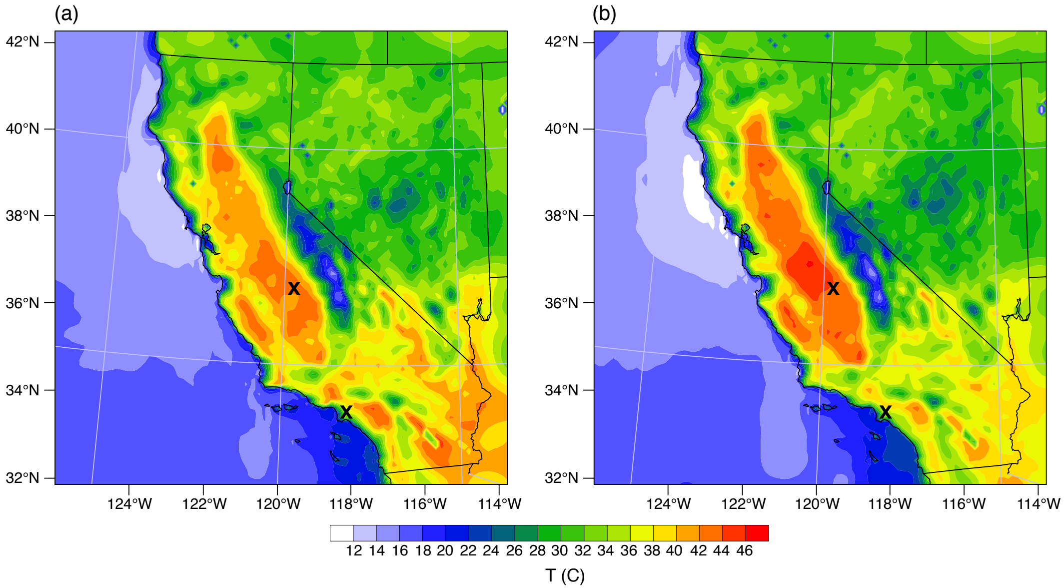

Fig. 1. Surface air temperature [°C] simulated by WRF for **(a)** 22 July 2006 and **(b)** 23 July 2006 over California and Nevada at 16:00 LT. Crosses show the sample locations in Los Angeles and the Central Valley used in Fig. 2.

ACPD
12, 23793–23828, 2012

Could aerosol emissions be used for regional heat wave mitigation?

D. N. Bernstein et al.

CC BY

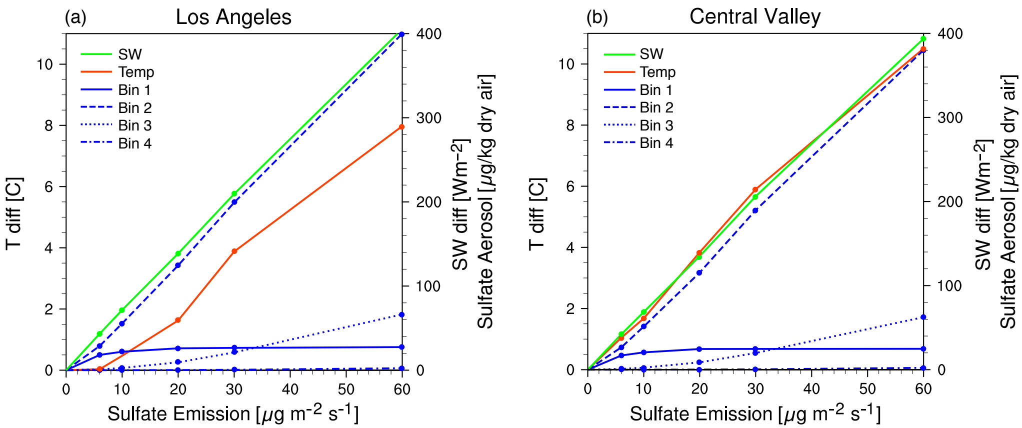

Fig. 2. Sulfate aerosol mixing ratio in each bin [$\mu g\,kg^{-1}$ of dry air] at the level of the injection with surface temperature [°C] and surface shortwave flux [$W\,m^{-2}$] differences as a function of the amplitude of sulfate aerosol emissions [$\mu g\,m^{-2}\,s^{-1}$] for the large-scale experiment at 13:00 LT on 22 July for **(a)** a point in Los Angeles and **(b)** a point in the Central Valley (Fresno). See Fig. 1 for point locations. See Sect. 2 for bin sizes, defined by dry particle diameter.

ACPD
12, 23793–23828, 2012

CC BY

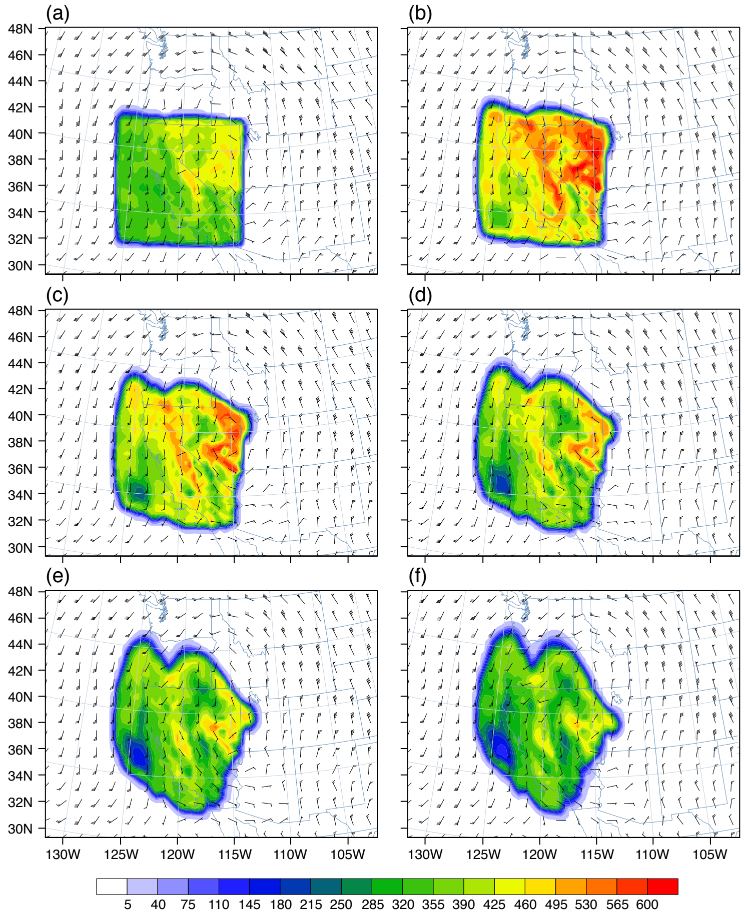

Fig. 3. Bin 2 (0.156–0.625 µm) sulfate aerosol mixing ratios [$\mu g\,kg^{-1}$ of dry air] and wind barbs (kts) at the level of the injection on 22 July at hours **(a)** 08:00 LT, **(b)** 10:00 LT, **(c)** 12:00 LT, **(d)** 14:00 LT, **(e)** 16:00 LT, and **(f)** 18:00 LT.

ACPD
12, 23793–23828, 2012

Title Page
Abstract | Introduction
Conclusions | References
Tables | Figures
◀| |▶
◀ ▶
Back | Close
Full Screen / Esc
Printer-friendly Version
Interactive Discussion

cc BY

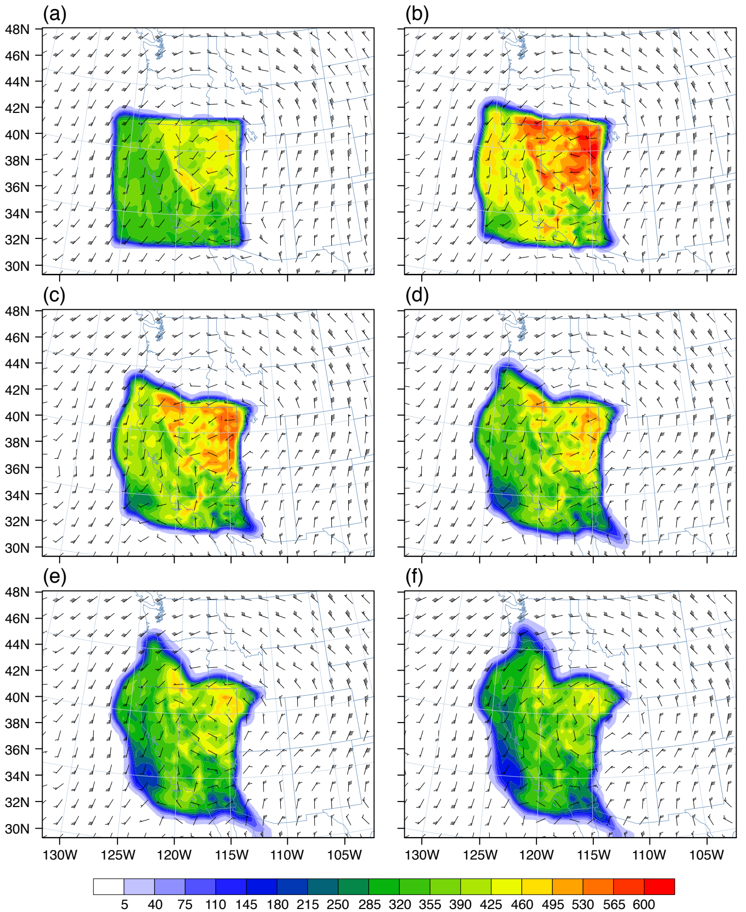

Fig. 4. Bin 2 sulfate aerosol mixing ratios [$\mu g\,kg^{-1}$ of dry air] and wind barbs (kts) at the level of the injection on 23 July at hours **(a)** 08:00 LT, **(b)** 10:00 LT, **(c)** 12:00 LT, **(d)** 14:00 LT, **(e)** 16:00 LT, and **(f)** 18:00 LT.

ACPD
12, 23793–23828, 2012

Could aerosol emissions be used for regional heat wave mitigation?

D. N. Bernstein et al.

Title Page
Abstract Introduction
Conclusions References
Tables Figures
◂ ▸
Back Close
Full Screen / Esc
Printer-friendly Version
Interactive Discussion

CC BY

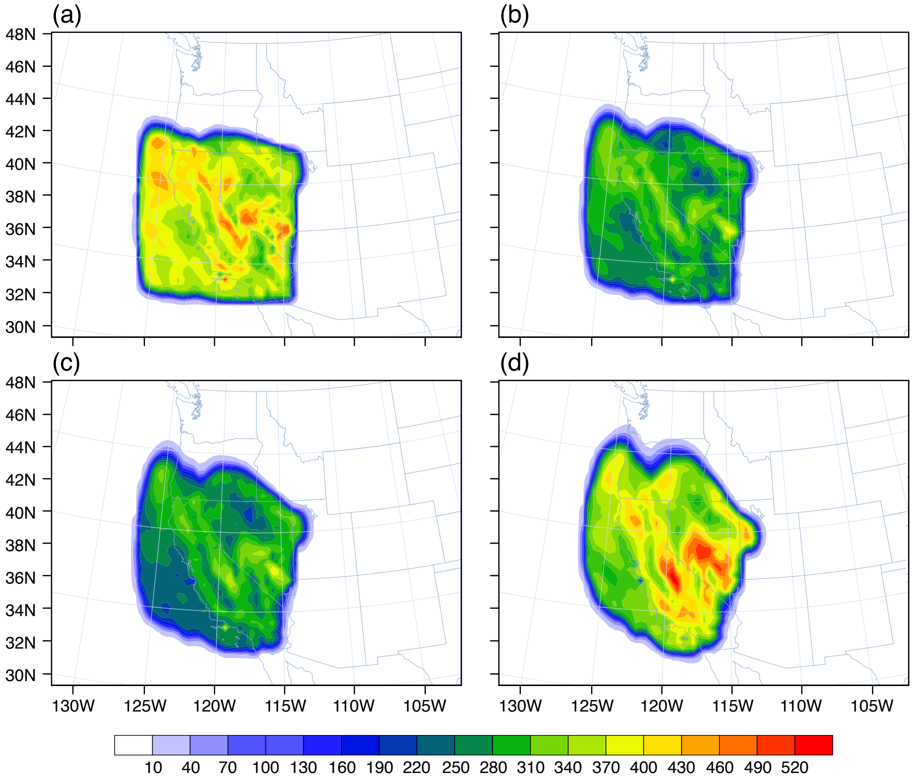

Fig. 5. Downward surface shortwave flux differences [$\mathrm{W\,m^{-2}}$] between large-scale $30\,\mu\mathrm{g\,m^{-2}\,s^{-1}}$ experiment and the control on 22 July at hours **(a)** 10:00 LT, **(b)** 12:00 LT, **(c)** 14:00 LT, and **(d)** 16:00 LT.

ACPD
12, 23793–23828, 2012

cc BY

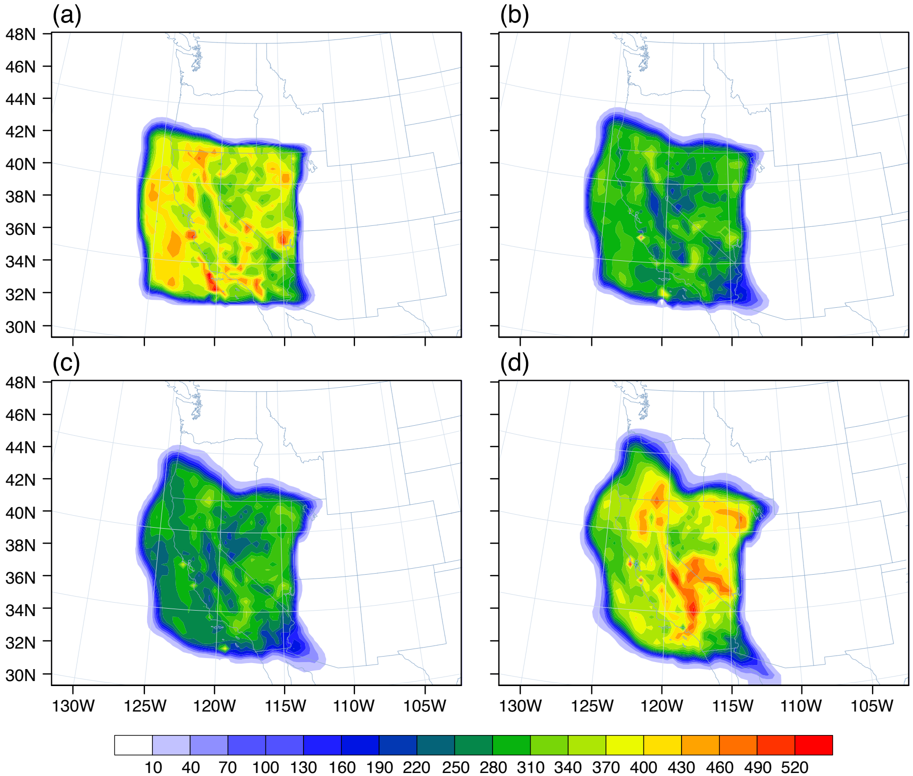

Fig. 6. Downward surface shortwave flux differences [$W m^{-2}$] between large-scale 30 $\mu g m^{-2} s^{-1}$ experiment and the control on 23 July at hours **(a)** 10:00 LT, **(b)** 12:00 LT, **(c)** 14:00 LT, and **(d)** 16:00 LT.

ACPD
12, 23793–23828, 2012

Could aerosol emissions be used for regional heat wave mitigation?

D. N. Bernstein et al.

cc BY

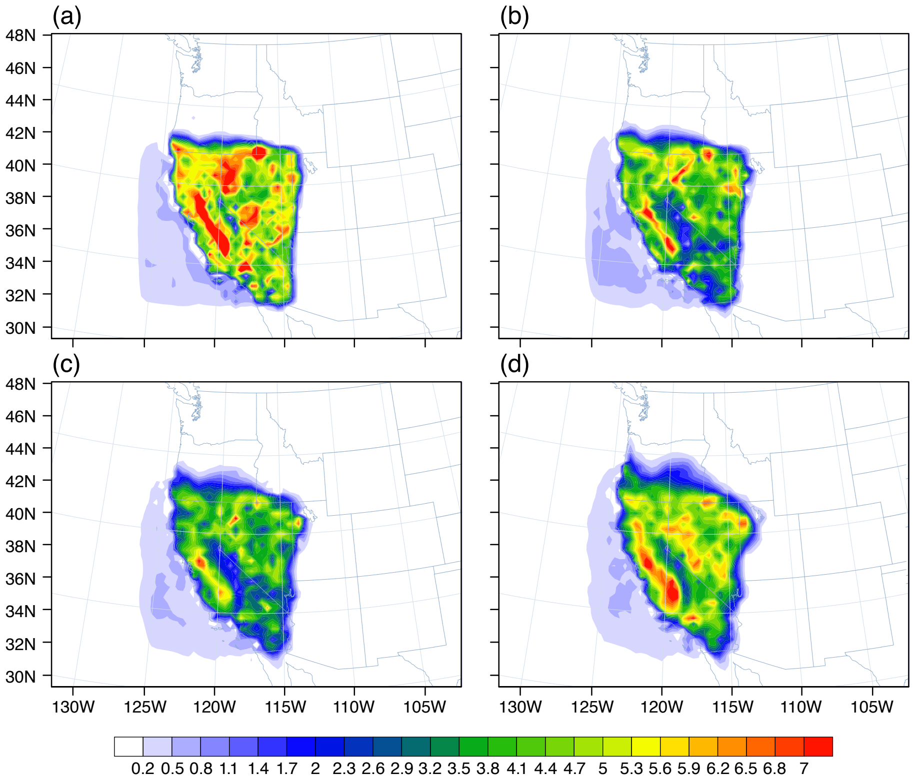

Fig. 7. Surface air temperature differences, [°C] between large-scale 30 µg m^{-2} s^{-1} experiment and the control on 22 July at hours **(a)** 10:00 LT, **(b)** 12:00 LT, **(c)** 14:00 LT, and **(d)** 16:00 LT.

ACPD
12, 23793–23828, 2012

CC BY

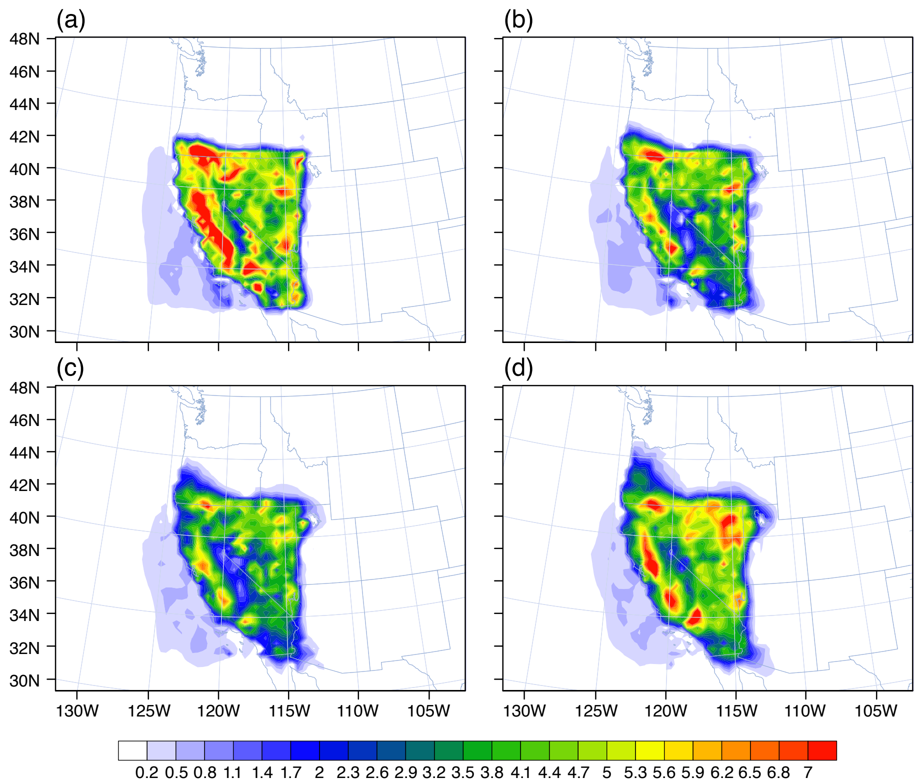

Fig. 8. Surface air temperature differences, [°C] between large-scale 30 μg m^{-2} s^{-1} experiment and the control on 23 July at hours **(a)** 10:00 LT, **(b)** 12:00 LT, **(c)** 14:00 LT, and **(d)** 16:00 LT.

ACPD
12, 23793–23828, 2012

Could aerosol emissions be used for regional heat wave mitigation?

D. N. Bernstein et al.

cc BY

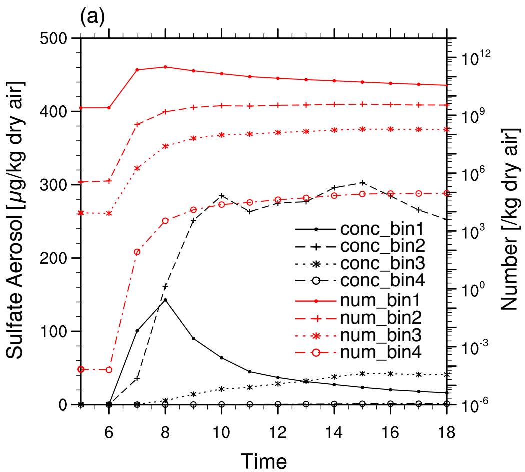

Fig. 9. Time-series (local time) of sulfate aerosol mixing ratio [$\mu g\,kg^{-1}$ dry air] (black) and aerosol number [kg^{-1} dry air] in each size bin (red) at the level of the injection for 22 July for a point locations **(a)** in Los Angeles and **(b)** in the Central Valley (Fresno). See Fig. 1 for point locations.

ACPD
12, 23793–23828, 2012

CC BY

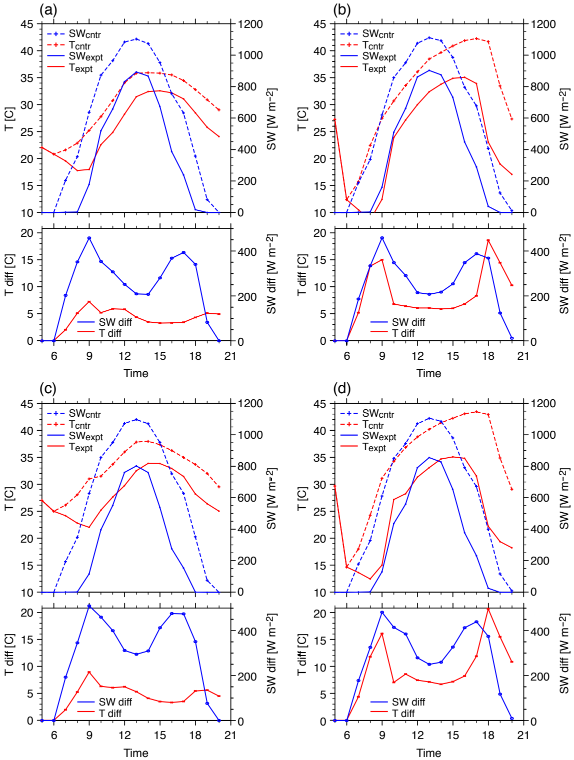

Fig. 10. Time-series (local time) of surface air temperature [°C] (red) and surface shortwave flux [W m^{-2}] (blue); the upper panel shows the control run and experimental surface air temperature and surface shortwave radiation flux, and the lower panel shows the differences between the control run and the experimental surface air temperature and surface shortwave radiation flux for **(a)** Los Angeles, 22 July, **(b)** Central Valley (Fresno), 22 July, **(c)** Los Angeles, 23 July, **(d)** Central Valley (Fresno), 23 July.

ACPD
12, 23793–23828, 2012

Title Page
Abstract | Introduction
Conclusions | References
Tables | Figures
◀| |▶
◀ ▶
Back | Close
Full Screen / Esc
Printer-friendly Version
Interactive Discussion

CC BY

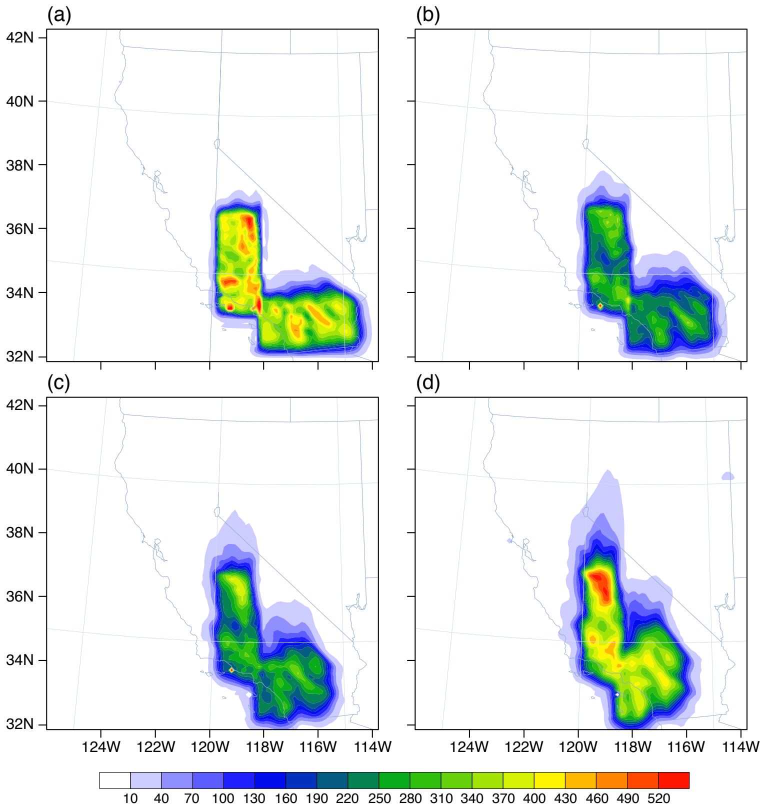

Fig. 11. Downward surface shortwave flux differences [$W m^{-2}$] on 22 July at hours **(a)** 10:00 LT, **(b)** 12:00 LT, **(c)** 14:00 LT, and **(d)** 16:00 LT for the smaller-scale injection experiments.

ACPD
12, 23793–23828, 2012

Could aerosol emissions be used for regional heat wave mitigation?

D. N. Bernstein et al.

Title Page
Abstract
Introduction
Conclusions
References
Tables
Figures
◀
▶
Back
Close
Full Screen / Esc
Printer-friendly Version
Interactive Discussion

CC BY

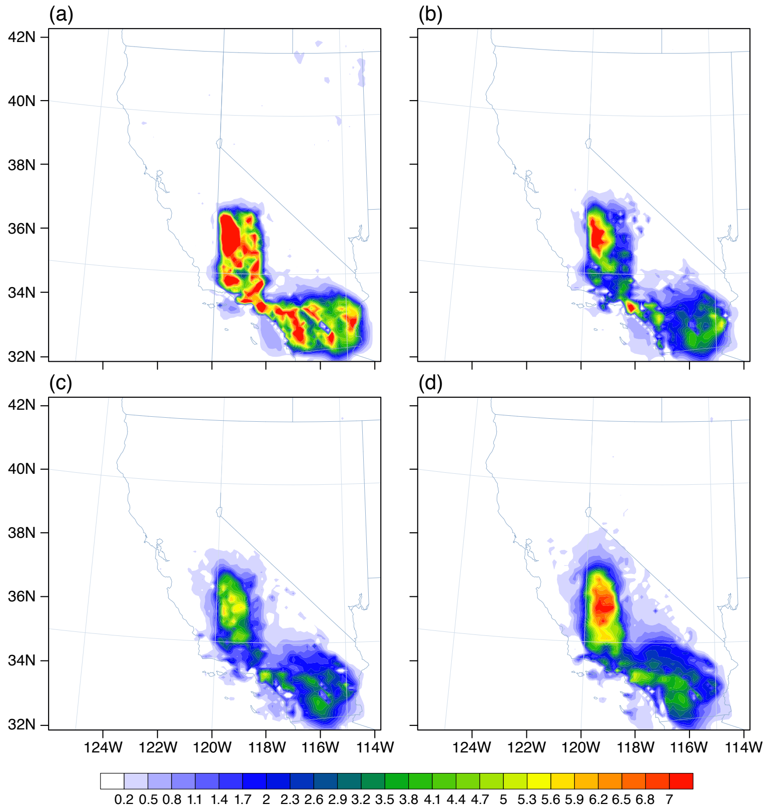

Fig. 12. Surface air temperature differences [°C] on 22 July at hours **(a)** 10:00 LT, **(b)** 12:00 LT, **(c)** 14:00 LT, and **(d)** 16:00 LT for the smaller-scale injection experiments.

ACPD
12, 23793–23828, 2012

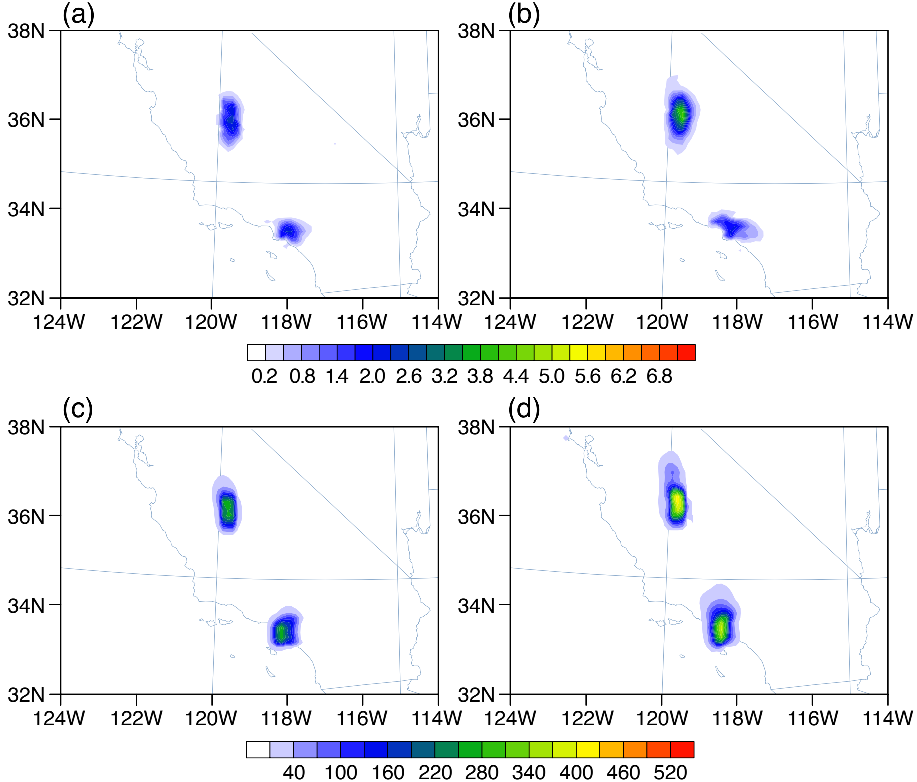

Fig. 13. **(a)** Surface air temperature differences [°C] for the metropolitan-size injection experiments on 22 July at 14:00 LT; **(b)** as in **(a)** but at 16:00 LT; **(c)** downward surface shortwave flux differences [$W m^{-2}$] on 22 July at 14:00 LT; and **(d)** as in **(c)** but for 16:00 LT.

ACPD
12, 23793–23828, 2012

Could aerosol emissions be used for regional heat wave mitigation?

D. N. Bernstein et al.

CC BY